NJC

PAPER

View Article Online
View Journal



Cite this: DOI: 10.1039/c5nj00324e

# Zinc hydroxide/oxide and zinc hydroxy stannate photocatalysts as potential scaffolds for environmental remediation†

Osmando F. Lopes,[ab] Vagner R. de Mendonça,[b] Ahmad Umar,[cd] Mohinder S. Chuahan,[e] Ramesh Kumar,[e] Suvarcha Chauhan[e] and Caue Ribeiro*[b]

This work describes the facile aqueous solution based syntheses and detailed characterization of zinc based hydroxide/oxide and zinc hydroxy stannate materials and their efficient utilization as catalyst for the photodegradation of harmful organic dye, *i.e.* Rhodamine B. The detailed studies revealed that the reaction time and temperature are important parameters by which the crystal phases and morphology of prepared materials can be controlled. Therefore, it was observed that with increasing the reaction time and temperature, a mixed phase of $Zn(OH)_2$ and ZnO and pure ZnO can be prepared. The detailed characterizations showed that zinc hydroxy stannate cubes grow in high density and possess cube shaped morphologies. The detailed photocatalytic experiments revealed that as-synthesized $ZnSn(OH)_6$ cubes possess higher photoactivity compared to the zinc based hydroxide/oxide materials. The stability results indicated no significant deactivation even after four successive re-uses in RhB photodegradation. Furthermore, the rate of •OH radical formation during UV irradiation was also tracked to investigate the mechanism of RhB photodegradation. The same trend was also observed on comparing the photoactivity and rate of •OH radical formation. Thus, it can be proposed that the mechanism of RhB degradation catalyzed by the as-synthesized materials followed an indirect oxidation of the dye by •OH radicals formed over the photocatalyst during UV irradiation, instead of direct electron transfer between dye and photocatalyst because there was no remarkable adsorption of the dye onto the photocatalyst surface.

Received (in Porto Alegre, Brazil) 6th February 2015,
Accepted 27th March 2015

DOI: 10.1039/c5nj00324e

www.rsc.org/njc



## 1. Introduction

The growth of the global population, coupled with economic development, has caused serious environmental problems such as contamination of drinking water by persistent organic pollutants.[1,2] Various methods for the treatment of aqueous organic waste have been studied, including the application of semiconductor as photocatalyst, which stands out because of its simplicity and high efficiency.[3–5]

Several semiconductor materials have been reported to be applicable in the photodegradation of pollutants.[6–8] Including oxides and sulfides, hydroxide materials possess band structure suitable to be applied as photocatalysts, but these materials have been neglected, in part due to their low stability.[9] Zinc oxide (ZnO, an n-type semiconductor with a direct band gap of 3.37 eV) is considered due to its slow recombination rate of charge carriers compared to other semiconductor oxides and suitable redox potential values of valence and conduction bands, which lead to reactions of interest in photocatalysis.[9–13]

In addition to zinc based hydroxides/oxides materials, zinc hydroxy stannate ($ZnSn(OH)_6$; ZHS), a non-toxic compound used as fire-retardant and smoke suppressant for various polymeric substrates, is also considered for photocatalysis.[14,15] ZHS is a semiconductor material with perovskite-structured hydroxide class and possesses band gap energies in the range of 3.2 to 4.3 eV.[16,17] Fu *et al.* have demonstrated the photocatalytic degradation of benzene using $ZnSn(OH)_6$ materials.[18] In another report, Fu *et al.* presented the photocatalytic reformation of ethanol to $H_2$ and $CH_4$ over ZHS cubes.[19] Thus, due to its remarkable properties and applications, ZHS was synthesized by various techniques such as solvothermal method,[18] sonochemical method,[20] co-precipitation method,[21] and hydrothermal method.[22] The presented methods to prepare ZHS materials require specific reaction conditions,

[a] Department of Chemistry-Federal University of São Carlos, Rod. Washington Luiz, km 235, 13565-905, São Carlos-SP, Brazil
[b] Embrapa Instrumentação, XV de Novembro 1452, 13560-970, São Carlos-SP, Brazil. E-mail: caue.ribeiro@embrapa.br
[c] Promising Centre for Sensors and Electronic Devices, Najran University, P.O. Box 1988, Najran, 11001, Kingdom of Saudi Arabia
[d] Department of Chemistry, Faculty of Sciences and Arts, Najran University, Najran University, P.O. Box 1988, Najran, 11001, Kingdom of Saudi Arabia
[e] Department of Chemistry, Himachal Pradesh University, Shimla-5, Himachal Pradesh, 171005, India

† Electronic supplementary information (ESI) available. See DOI: 10.1039/c5nj00324e

chemicals and instruments. Thus, it is necessary to develop a simple, facile and effective low-temperature method to synthesize good quality ZHS materials.

In this sense, this paper reports simple and facile aqueous solution based low-temperature syntheses of zinc based hydroxide/oxide and zinc hydroxy stannate materials in large quantity. The as-synthesized materials were characterized in terms of their morphological, structural and compositional properties. Furthermore, the prepared materials were used as photocatalysts for the photodegradation of Rhodamine B under UV irradiation. Finally, to investigate the mechanisms underlying the photodegradation of dye, the rate of hydroxyl radical formation under UV irradiation was also studied and presented in this paper.

## 2. Experimental details

### 2.1. Materials

All the chemicals were used as received without further purifications. Zinc nitrate hexahydrate ($Zn(NO_3)_2{\cdot}6H_2O$), tin chloride dihydrate ($SnCl_2{\cdot}2H_2O$), ammonium hydroxide (NaOH) and Rhodamine B (RhB) were purchased from Sigma-Aldrich, and ethylenediamine (en) was supplied by E. Merck. For all the experiments, de-ionized (DI) water was used.

### 2.2. Synthesis of zinc based hydroxide/oxide photocatalysts

Zinc based hydroxide/oxide materials were synthesized by a simple and facile aqueous solution approach at a low temperature. Three samples were prepared; *i.e.* almost pure $Zn(OH)_2$, hereafter called as Zn-1; mixed $Zn(OH)_2$ and ZnO referred to as Zn-2 and pure ZnO denoted as Zn-3. For the synthesis of Zn-1, in a typical reaction process, 0.1 mol $L^{-1}$ $Zn(NO_3)_2{\cdot}6H_2O$ was prepared in 100 mL DI water, which was mixed well with 0.1 mol $L^{-1}$ ethylenediamine with continuous stirring. The stirring was continued for 10 min. The pH of the resulting solution was maintained at 11 by adding a few drops of $NH_4OH$ solution. The final solution was then heated and refluxed at 55 °C for 1 h. The same reaction procedure was repeated to prepare Zn-2 and Zn-3 samples; however, the temperature and reaction time were varied. To prepare Zn-2, the reaction mixture was refluxed and heated at 70 °C for 5 h, while Zn-3 sample was synthesized at 85 °C for 10 h. After completing the reaction, the mixture was allowed to cool at room temperature. The obtained white colored precipitates were collected after repeatedly washing with DI water and finally with ethanol, and they were left to dry at room temperature in air.

### 2.3. Synthesis of zinc hydroxy stannate cubes

Large-quantity synthesis of zinc hydroxy stannate ($ZnSn(OH)_6$; ZHS) cubes was successfully done by a simple and facile aqueous solution method. In a typical reaction process, 0.3 mol $L^{-1}$ $Zn(NO_3)_2{\cdot}6H_2O$, 0.3 M ethylenediamine and 0.03 mol $L^{-1}$ $SnCl_2{\cdot}2H_2O$, all prepared in 100 mL DI water each, were mixed well under continuous stirring. To maintain the pH at 11, a few drops of $NH_4OH$ were added in the resultant solution. The obtained solution was then further stirred for 30 min. After stirring, the final obtained solution was heated and refluxed at 95 °C for 12 h. After the completion of the reaction, the mixture was allowed to cool at room-temperature. The obtained grayish-white colored precipitates were collected after repeatedly washing with DI water and ethanol, and the materials were left to dry in a hot air oven.

### 2.4. Characterizations of as-synthesized samples

The crystallinity and phase identifications of the prepared samples were examined by X-ray powder diffraction (XRD; Shimadzu XRD-6000) at 30 kV and 30 mA with Cu-K$\alpha$ radiation in the range of $2\theta$ = 10–75°. A field emission gun-scanning electron microscope (FEG-SEM JEOL JSM 6701F) operating at 2.0 kV was used to observe the morphologies of as-synthesized materials. High resolution transmission electron microscopy (HRTEM; TECNAI F50) operating at 200 kV was used to verify the morphology and crystallographic orientations. The scattering properties were examined by Raman-scattering spectroscopy (Horiba Jobin-Yvon Raman spectrometer coupled to an Olympus TM BX41 microscope) using a 514.5 nm argon laser. The chemical compositions were evaluated by Fourier transform infrared absorption spectroscopy (FTIR-PerkinElmer Spectrum 1000). The analysis of $N_2$ adsorption at 77 K was conducted in a Micrometrics ASAP 2000, and the specific surface area was obtained by applying the BET modeling. To obtain the band gap of the as-synthesized samples, UV-vis diffuse reflectance spectra were recorded on a Varian model Cary 5G spectrometer from 200 to 800 nm using the Tauc method for the calculation. The measurements were performed in the total reflection mode with an integration cell containing MgO powder.

### 2.5. Photocatalytic performance evaluation

The photocatalytic activity in terms of the oxidation of RhB dye was tested under UV illumination. All the experiments were performed in a photoreactor at a controlled temperature (18 °C) using a UVC radiation source (Lamps Phillips TUV, 15 W; maximum intensity = 254 nm). The powder of the as-synthesized materials (150 mg $L^{-1}$) was dispersed in aqueous RhB solution (5.0 mg $L^{-1}$). The solutions were kept in the dark for 12 h before the photocatalytic tests to evaluate possible adsorption. However, none of the samples showed significant adsorption. To evaluate the photocatalytic performances, UV light was irradiated over the resultant solution for various time intervals and the absorbance was measured using a UV-vis spectrophotometer. At regular time intervals, the samples were collected and analyzed in a UV-vis spectrophotometer (Shimadzu-1601PC) in the absorbance mode, monitoring RhB degradation kinetics at 554 nm.

The reuse of the ZHS cubes was also investigated. After each reaction cycle, the photocatalyst was separated from the RhB solution by centrifugation. Then, a new solution was placed in contact with the used photocatalyst, and the following reaction was performed four times. For this test, 500 mg $L^{-1}$ of ZHS in RhB solution (5.0 mg $L^{-1}$) was used for 4 h.

To investigate the mechanism underlying the RhB photodegradation, analyses of the rate of hydroxyl radical formation were also performed.[23] The experiments were performed indirectly through the detection of 2-hydroxyterephthalic acid formed by the reaction of hydroxyl radicals with terephthalic acid

 

(TPA-Aldrich, 98% pure). For this experiment, particles were dispersed in a solution of terephthalic acid at a concentration of $4 \times 10^{-4}$ mol $L^{-1}$, prepared in NaOH ($2 \times 10^{-3}$ mol $L^{-1}$). The suspension was irradiated using the same conditions of photodegradation tests and $^{\bullet}OH$ radical formation was evaluated by measuring the change of fluorescence intensity emitted from 2-hydroxyterephthalic acid at 425 nm when excited at 315 nm in a Perkin Elmer LS 50B fluorescence spectrometer.

## 3. Results and discussion

### 3.1. Detailed characterizations of zinc based hydroxide/oxide photocatalyst

The crystallinity and crystal phases of the as-prepared zinc based hydroxide/oxide materials were characterized by X-ray diffraction pattern, and results are shown in Fig. 1(a). In the XRD patterns for Zn-1 and Zn-2 samples, several well-defined diffraction reflections, which are related to the mixed phases of zinc hydroxide, $Zn(OH)_2$ and ZnO, are seen. The observed diffraction reflections are consistent with the PDF # 01-089-0138 and 01-080-0075 for $Zn(OH)_2$ and ZnO, respectively. Interestingly, it was observed that, with increasing reaction temperature and time, the intensities of $Zn(OH)_2$ reflections were decreased and ZnO reflections were increased. This phenomenon confirms that the longer reaction time and higher reaction temperature are important for the conversion of $Zn(OH)_2$ to ZnO. With further increasing the reaction time to 10 h and the temperature to 85 °C, pure ZnO powder was obtained, as confirmed by the observed XRD pattern for Zn-3, which exhibits several well-defined diffraction reflections that are related with pure wurtzite hexagonal phase ZnO. The results clearly confirmed that pure ZnO materials can be synthesized by optimizing the reaction conditions to appropriate reaction time and temperature.

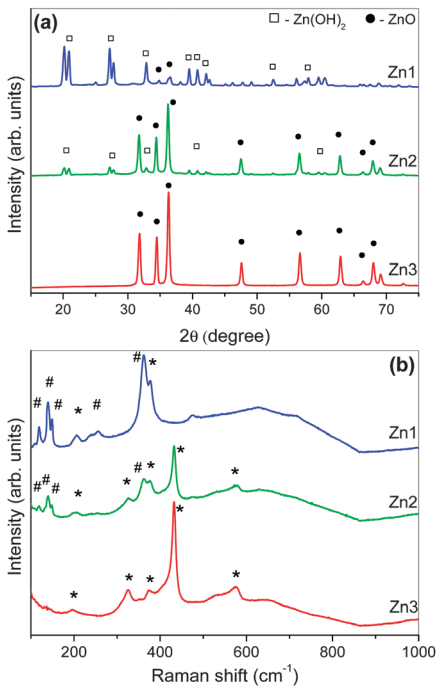


Fig. 1 (a) Typical XRD patterns of the as-synthesized zinc based hydroxide/oxide samples. In the pattern, (□) is identified as $Zn(OH)_2$ and (●) is identified as ZnO. (b) Raman spectra of Zn-1, Zn-2 and Zn-3 samples. In the spectra, (#) is identified as $Zn(OH)_2$ and (*) is identified as ZnO.

Furthermore, because the Raman-scattering technique is believed to be more sensitive than XRD analysis for analyzing the phase mixtures of prepared materials, the materials were also analyzed by Raman-scattering spectroscopy at room-temperature, and the results are shown in Fig. 1(b). In the spectrum of Zn-1 sample, several well-defined peaks are observed at 120, 141, 151, 259 and 361 $cm^{-1}$, which can be assigned to translational modes (Zn–O). All these peaks are related to zinc hydroxide and marked as '#'. The observed zinc hydroxide peaks are similar to those reported in the literature.[24] Furthermore, two small peaks at 206 and 378 $cm^{-1}$ are also seen in the spectrum, which can be assigned as vibrational modes $M_1$ and $A_1$ (TO). These small peaks are related with the wurtzite hexagonal phase of ZnO and marked as '*' in the spectrum. The observed Raman-scattering result suggests that the as-synthesized Zn-1 sample is the mixture of $Zn(OH)_2$ and ZnO. The observed result is fully consistent with XRD results.

In addition to the peaks that appear for Zn-1, Zn-2 sample exhibited additional peaks at 331, 437 and 580 $cm^{-1}$, which are related with the wurtzite hexagonal ZnO and can be assigned as $M_2$, $E_2^{high}$ and $A_1$ (LO), respectively. It is clear from the observed spectrum that the peak intensities of $Zn(OH)_2$ phases are decreased, while the intensities for ZnO related phases are increased. This clearly reflects that with increasing reaction temperature and time, $Zn(OH)_2$ changes to ZnO, and Zn-2 sample possess higher amounts of ZnO compared to Zn-1 sample.

The Raman-scattering spectrum of Zn-3 sample reveals several well-defined peaks at 204, 331, 379, 437, 540, 580, and 661 $cm^{-1}$. The peaks appearing at 379, 437 and 580 $cm^{-1}$ are assigned to the vibration modes of $A_1$ (TO), $E_2^{high}$ and $A_1$ (LO) optical phonons, respectively. Moreover, additional modes ($M_1$ to $M_4$) at 204, 331, 540 and 661 $cm^{-1}$ are assigned to overtones and combinations.[25,26] All the observed peaks in the Raman-scattering spectrum of Zn-3 sample are efficiently matching the typical pure wurtzite hexagonal phase ZnO. All the observed Raman-scattering results are consistent with the XRD observations of zinc based hydroxide/oxide.

The general morphologies of as-synthesized zinc based hydroxide/oxide were examined by FEG-SEM analysis, and the results are shown in Fig. 2(a) and (b). The as-synthesized zinc based hydroxide/oxide exhibit the typical FEG-SEM images of as-synthesized sample Zn-1 and revealed that the synthesized $Zn(OH)_2$ materials possess flake-shaped morphologies, which are considerably agglomerated with flakes stacked upon each other.

Fig. 2(c) and (d) exhibit the typical FEG-SEM images of Zn-2 sample and confirmed that the grown structures are broken small rods. Interestingly, the broken rods exhibited perfectly hexagonal surfaces and facets throughout their lengths, typical of hexagonal ZnO. Sample Zn-3 exhibits large-quantity growth of perfectly hexagonal-shaped pure ZnO rods (Fig. 2(e) and (f)). The rods possess sharp tips and wider bases. In addition to

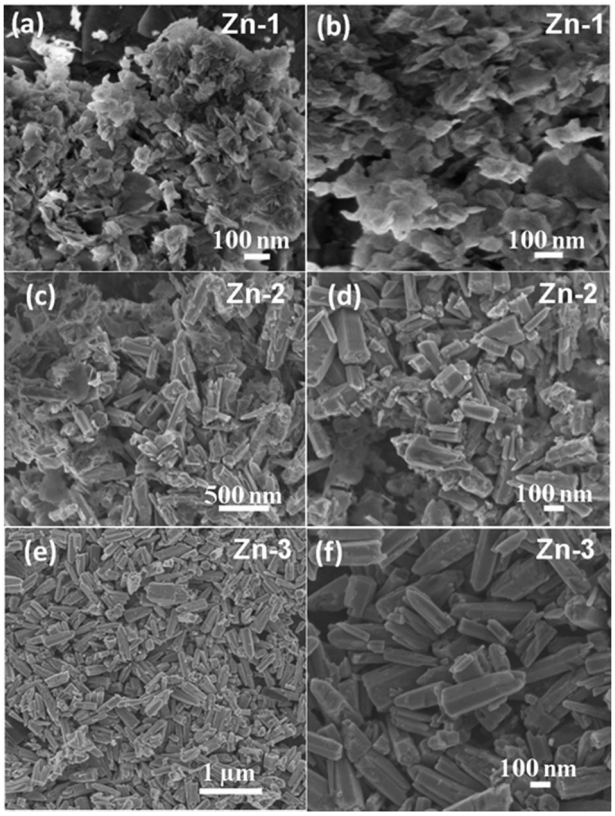


Fig. 2 Typical FEG-SEM images of as-synthesized zinc based hydroxide/oxide samples; (a and b) Zn-1; (c and d) Zn-2; and (e and f) Zn-3.

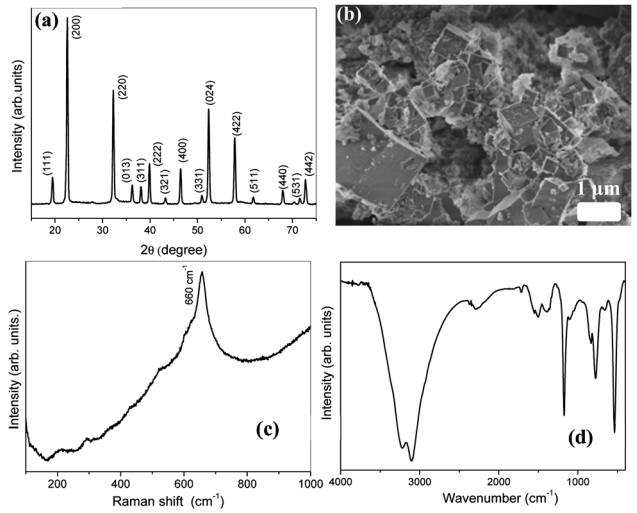


Fig. 3 Typical (a) XRD pattern, (b) SEM images; (c) Raman-scattering spectrum and (d) FTIR spectrum of as-synthesized zinc hydroxy stannate cubes.

well-defined rods, some broken rods were also seen in the micrograph. The perfect hexagonal morphologies of rods confirmed that the prepared material possesses wurtzite hexagonal phase.

### 3.2. Detailed characterizations of zinc hydroxy stannate (ZHS) cubes

Fig. 3(a) exhibits the typical XRD pattern of the as-synthesized ZHS cubes. The measured XRD pattern exhibits various well-defined diffraction reflections that are related to the cubic phase of $ZnSn(OH)_6$ with a cell edge of 7.80 Å and space group *Pn*3*m* (PDF # 20-1455).

The general morphologies of as-synthesized ZHS materials were examined by SEM, and results are demonstrated in Fig. 3(b). As can be seen from the observed SEM images, the synthesized material possesses cubic morphologies. The synthesized cubes are grown in large quantity with edge lengths around 500 nm. Furthermore, the scattering properties of as-synthesized ZHS cubes were examined by Raman-scattering spectroscopy, and the results are shown in Fig. 3(c). Only a sharp and strong Raman-scattering peak at 660 $cm^{-1}$ appeared in the observed spectrum, which is related to the cubic phase, $ZnSn(OH)_6$ (identified by Rocklin Residents Unite For Fido, RRUFF, ID number R070216).[27] Fig. 3(d) depicts the typical FTIR spectrum of the as-synthesized ZHS cubes. Clearly, the FTIR spectrum exhibited a shift at 3200 $cm^{-1}$, which is assigned to Sn–OH bonds. This is noteworthy because in the other samples (see Fig. S1 at ESI†), the bonds are diffused, which may refer to a disordered linkage of water and OH groups over the surface. The FTIR spectrum also shows a sharp peak at 1174 $cm^{-1}$, which may arise due to Sn–OH bending, while the peak appearing at 775 $cm^{-1}$ may be attributed to water hydrogen bonding. The origination of a sharp peak at 540 $cm^{-1}$ is due to the Sn–O stretching mode.[28]

The detailed morphological properties of as-synthesized ZHS cubes were examined by transmission electron microscopy (TEM) equipped with high-resolution TEM (HRTEM). Fig. 4(a)–(c) exhibit the typical low-magnification TEM images of as-synthesized ZHS cubes. It is clear from the observed TEM images that the prepared material possesses a cube shape and grows in high density. The typical sizes of the cubes were around 500 nm; however, some size deviations were also seen in the micrographs. The cubes exhibited sharp edges, as confirmed from Fig. 4(c).

Interestingly, similar to the SEM analysis, it was seen that some flask-shaped morphologies, made of small particles, are also attached on the outer surface of the cubes. Fu *et al.* have explained that the formation of such flakes and particles on the outer surfaces of ZHS cubes are most probably due to the adsorption of small particles, as observed for $In(OH)_3$ cubes.[18,29] Fig. 4(d) exhibits the HRTEM image of the flake-shaped particles. The interplanar distance of 1.15 nm cannot be assigned to any ZHS phase planes, as previously proposed.[18,29] Probably, this distance is related to a meso-organization of lamellar structure, given as a precursor of cubic morphology. Fig. 4(e) shows the HRTEM image of small particles (flake-shaped), which are also attached on the outer surface of the cubes; this confirms the growth mechanism of cubes by the adsorption of small particles.

### 3.3. Photocatalytic degradation of Rhodamine B using zinc based hydroxide/oxide structures and ZHS cubes

The as-synthesized zinc based hydroxide/oxide and zinc hydroxy stannate structures were used as catalysts for the photodegradation of RhB under UV irradiation, and the results are shown

 

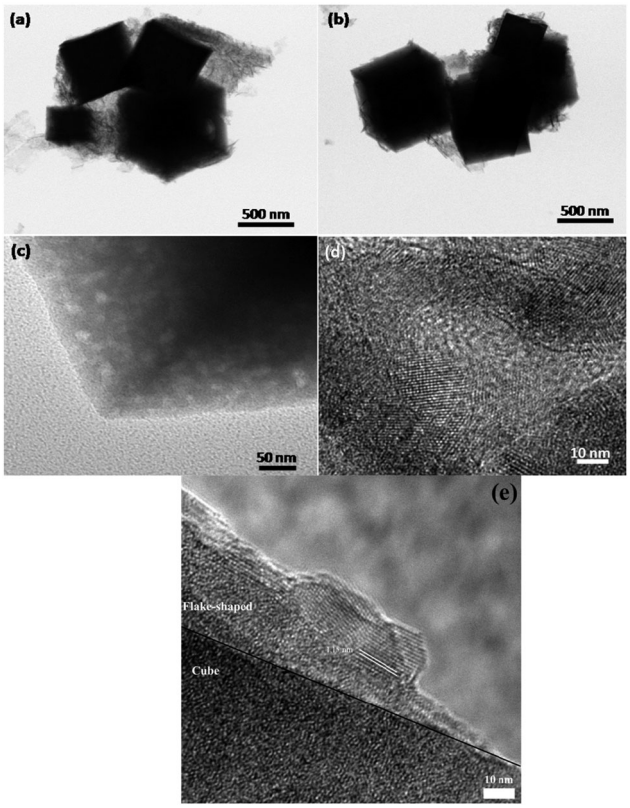


Fig. 4 Typical (a and b) low-magnification and (c, d and e) high-resolution TEM images of as-synthesized zinc hydroxy stannate cubes.

in Fig. 5(a). RhB photolysis was evaluated without any catalyst and nearly 10% of RhB was degraded after 3 h of irradiation. It is important to mention that there was no adsorption of the dye onto the photocatalyst surface, indicating that direct dye oxidation is not taking place in the experiments. Fig. 5(b) exhibits the first-order kinetics plot for RhB photodegradation, where the slope of the line is the pseudo-order rate constant ($k'$). The values of $k'$ are presented in Table 1.

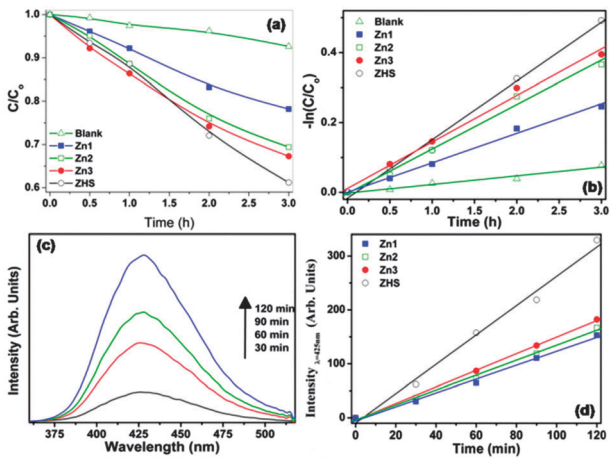


Fig. 5 (a) Photodegradation kinetics of RhB under UV light (254 nm); (b) First-order kinetics plot for RhB photo-degradation; (c) the spectra profile of 2-hydroxyterephthalic acid and (d) Plot of spectrum intensity at 425 nm for each sample in different times of UV exposure.

Table 1 Specific surface area (SSA) and band gap of as-synthesized zinc hydroxide/oxide and zinc hydroxy stannate structures. Pseudo first-order rate constants for the RhB photo-degradation tests ($k'$) and $k_{OH}$•

| Sample | $E_g$ (eV) | SSA ($m^2\ g^{-1}$) | $k'$ ($h^{-1}$) | $k_{OH}$ ($min^{-1}$) |
|---|---|---|---|---|
| Zn-1 | 2.94 | 33.8 | 0.08 | 1.28 |
| Zn-2 | 3.08 | 15.1 | 0.127 | 1.38 |
| Zn-3 | 3.18 | 4.6 | 0.133 | 1.53 |
| ZHS | 3.22 | 38.3 | 0.167 | 2.71 |

The photoactivities towards RhB degradation for the prepared zinc based hydroxide/oxide and zinc hydroxy stannate structures could be related to the synthesis conditions. The samples containing higher amounts of $Zn(OH)_2$, such as Zn-1, showed lower photoactivity, followed by samples such as Zn-2, which contain higher amount of ZnO compared to the previous one, and Zn-3, which is pure ZnO. This trend is related to the amount of ZnO phase, which is known to be a better photocatalyst than $Zn(OH)_2$. However, the prepared ZHS cubes exhibited highest photoactivity, and thus despite its larger band-gap, it presents itself as a potential candidate to be applied as an effective photocatalyst for the photodegradation of various harmful dyes and pigments.

The photoactivity order observed can be explained as the sum of two effects: specific surface area and electronic properties (band gap). Band gap values were obtained applying the Tauc model to the data obtained from UV-vis diffuse reflectance spectroscopy (see Fig. S2 at ESI†), and the values are shown in Table 1. The band gap values found are in agreement with those reported in the literature for each phase.[2,16] It can be observed that the Zn-1 and Zn-2 samples presented band gap values of 2.94 and 3.08, respectively, this confirms that the minor activity of the sample containing $Zn(OH)_2$ phase compared to that of the ZnO phase is due to inadequate electronic properties (unsuitable redox potential of valence and/or conduction band). The Zn-3 and ZHS samples showed band gap values of 3.18 and 3.22, respectively, which are in accordance with other work, and they possess suitable electronic properties to cause redox reactions for the degradation of organic pollutants.[9–13,30]

Another important parameter for photocatalytic results observed was total available surface area for as-synthesized samples.[23,31] It is noticed that phase formation influenced this parameter because from samples Zn-1 to Zn-3, a remarkable reduction of SA was observed (Table 1). However, it is also important that the photoactivity was improved even in the SA reduction, which means that the ZnO phase was more active than the hydroxide forms (mainly due to the suitable electronic properties of ZnO phase). Moreover, the zinc hydroxy stannate formation improved the surface area, returning to values comparable to the Zn-1 sample. This means that the improvement in the photocatalytic activity of this sample may be explained by a sum of two parameters, *i.e.* suitable electronic properties and higher specific surface area.

The photodegradation of organic compounds in a heterogeneous process can occur by two main mechanisms. First, direct oxidation occurs when a pollutant initially adsorbs over the semiconductor surface; subsequently, the hole formed will

migrate to the surface of the material and oxidize the adsorbed pollutant. In indirect oxidation, the electron–hole pair acts to form free radicals from surface groups, such as M–OH, $O_2$, and adsorbed water. The formed radical species are generally $^{\bullet}OH$, $HO_2^{\bullet}$ and $O_2^{\bullet-}$, which are able to oxidize organic compounds in solution.[23,31]

Therefore, to investigate the photodegradation mechanism, the rate of $^{\bullet}OH$ radical formation over a photocatalyst surface during UV radiation was tracked for all the samples studied, and the results are depicted in Fig. 5(c) and (d). Considering a zero order kinetic ($[^{\bullet}OH]_t = k_{OH^{\bullet}}t$) for the reaction of hydroxyl radical formation over a semiconductor surface, the plot of the intensity at 425 nm against the irradiation time should be linear and the slope of the curve should be directly proportional to the rate of hydroxyl radical formation (Table 1).[23] Interestingly, the analysis followed the same trend as compared to the photoactivity of the samples, showing the relation between the photodegradation of the dye and hydroxyl radical formation. Finally, it can be observed that both kinetic constants ($k'$ and $k_{OH}$) follow the same trend. Therefore, we can conclude that attack by $^{\bullet}OH$ radical and dye oxidation, *i.e.* an indirect photodegradation mechanism, is the main photodegradation process.[23] This result is in agreement with the studies reported by Kumari *et al.*, who evaluated the photodegradation mechanism of RhB dye by zinc stannate ($Zn_2SnO_4$ and $ZnSnO_3$) under UV light.[32]

From these results, it is possible to infer that the zinc hydroxy stannate structure influences the reactivity of zinc sites with adsorbed OH groups because the FTIR results demonstrate the linkage of OH to Sn sites, and thus it is possible that both Zn and Sn sites were active in the photocatalytic process. This is a remarkable observation because Sn sites are generally inactive. It is known that $SnO_2$ sites do not exhibit significant photocatalytic activity most likely due to the relative position of (reduction potential) its conduction band, which is insufficient for reducing molecular oxygen ($O_2 + e^- \rightarrow {}^{\bullet-}O_2$ $E = -0.33$ eV).[31] In addition, it is well known that Sn and Sn oxides when coupled with the other oxides can improve photoactivity by acting as dopant or forming heterostructures.[33] However, it is possible that in perovskite-structured ZHS, Sn sites can be active, *i.e.*, the Sn sites can have sufficient redox potential to promote $O_2$ reduction, and thus improve ZHS photoactivity.

The cyclic stability results are shown in Fig. 6. These results indicated that no significant deactivation was observed with ZHS cubes even after four successive re-uses for RhB photodegradation. Therefore, the prepared ZHS cubes exhibit stable photocatalytic properties and an insignificant photocorrosion process, which is a problem generally associated with Zn compounds.[34,35]

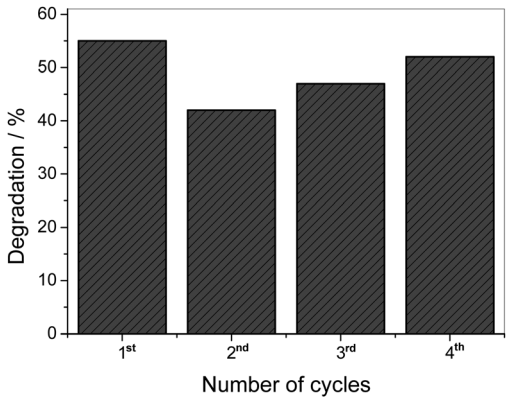


Fig. 6 Degradation percentage of RhB, *i.e.*, photocatalytic efficiency for the ZHS sample during the four cyclic stability tests.

## 4. Conclusion

In summary, zinc based hydroxide/oxide and zinc hydroxy stannate structures were synthesized by a facile aqueous solution process at a low temperature. It was investigated that by controlling the reaction parameters, mixed phases of $Zn(OH)_2$ and ZnO, pure ZnO and $ZnSn(OH)_6$ structures can be prepared. All the synthesized materials were used as photocatalysts for the photocatalytic degradation of RhB under UV-light irradiation. The most active photocatalyst, among all the prepared samples, was found to be $ZnSn(OH)_6$. Furthermore, the RhB photodegradation mechanism could be correlated to the attack of hydroxyl radicals formed during UV irradiation, instead of the direct oxidation of dye over the photocatalyst surface. Finally, the as-prepared $ZnSn(OH)_6$ cubes presented themselves as potential material for the efficient photodegradation of organic dyes and pigments with high stability.

## Acknowledgements

The authors thank FAPESP (project no. 13/13888-0 and 2009/54216-9), CNPq, CAPES and FINEP for the financial support. We are also grateful to LCE-DEMa and LIEC/UFSCar Brazil for providing HRTEM and Raman spectroscopy facilities, respectively. R. Kumar would like to thank the Council of Scientific and Industrial Research (CSIR), New Delhi, India for the awarding Senior Research Fellowship.

## Notes and references

1 H. A. J. L. Mourão, W. Avansi, J. E. Oliveira, E. S. Firmiano and C. Ribeiro, *Sci. Adv. Mater.*, 2013, **5**, 71.
2 T. M. Milão, V. R. de Mendonça, V. D. Araújo, W. Avansi, C. Ribeiro, E. Longo and M. I. Bernardi, *Sci. Adv. Mater.*, 2012, **4**, 54.
3 M. A. Gondal, M. A. Dastageer, S. G. Rashid, S. M. Zubair, M. A. Ali, D. H. Anjum, J. H. Lienhard, G. H. McKinley and K. Varanasi, *Sci. Adv. Mater.*, 2013, **5**, 2007.
4 M. Wang, Y. Gao, L. Dai, C. Cao, Z. Chen and X. Guo, *Sci. Adv. Mater.*, 2013, **5**, 1867.
5 G. R. Chaudhary, P. Saharan, A. Umar, S. K. Mehta and S. Mor, *Sci. Adv. Mater.*, 2013, **5**, 1886.
6 K. Nakata and A. Fujishima, *J. Photochem. Photobiol., C*, 2012, **13**, 169.
7 S. S. Arbuj, R. R. Hawaldar, S. Varma, S. B. Waghmode and B. N. Wani, *Sci. Adv. Mater.*, 2012, **4**, 568.

 

8 S. Martha, D. P. Das, N. Biswal and K. M. Parida, *J. Mater. Chem.*, 2012, **22**, 10695.
9 X. Fu, D. Huang, Y. Qin, L. Li, X. Jiang and S. Chen, *Appl. Catal., B*, 2014, **148–149**, 532.
10 J. M. Mali, S. S. Arbuj, J. D. Ambekar, S. B. Rane, U. P. Mulik and D. P. Amalnerkar, *Sci. Adv. Mater.*, 2013, **5**, 1994.
11 *Metal oxide nanostructures and their applications*, ed. A. Umar and Y. B. Hahn, American Scientific Publishers, Los Angeles, 2010.
12 S. K. Kansal, A. H. Ali, S. Kapoor and D. W. Bahnemann, *Sci. Adv. Mater.*, 2013, **5**, 630.
13 Y. H. Luo, J. Huang and I. Ichinose, *J. Am. Chem. Soc.*, 2005, **127**, 8296.
14 Z. Wang, J. Liu, F. Wang, S. Chen and H. Luo X. Yu, *J. Phys. Chem. C*, 2010, **114**, 13577.
15 C. Liu, R. Roder, L. Zhang, Z. Ren, H. Chen, Z. Zhang, C. Ronning and P. X. Gao, *J. Mater. Chem. A*, 2014, **2**, 4157.
16 W. Wang, Z. Ma, R. Liang, T. Wu and Y. Wu, *J. Mater. Res.*, 2013, **28**, 1582.
17 L. Wang, K. Tang, Z. Liu, D. Wang, J. Shang and W. Cheng, *J. Mater. Chem.*, 2011, **21**, 4352.
18 X. Fu, X. Wang, Z. Ding, D. Y. C. Leung, Z. Zhang, J. Long, W. Zhang, Z. Li and X. Fu, *Appl. Catal., B*, 2009, **91**, 67.
19 X. Fu, D. Y. C. Leung, X. Wang, W. Xue and X. Fu, *Int. J. Hydrogen Energy*, 2011, **36**, 1524.
20 H. Jena, K. V. G. Kutty and T. R. N. Kutty, *Mater. Chem. Phys.*, 2004, **88**, 167.
21 L. C. Basciano, R. C. Peterson, P. L. Roeder and I. Swainson, *Can. Mineral.*, 1998, **36**, 1203.
22 J. Zeng, M. D. Xin, K. W. Li, H. Wang, H. Yan and W. J. Zhang, *J. Phys. Chem. C*, 2008, **112**, 4159.
23 O. F. Lopes, E. C. Paris and C. Ribeiro, *Appl. Catal., B*, 2014, **144**, 800.
24 H. D. Lutz, C. Jung, R. Mortel, H. Jacobs and R. Stahl, *Spectrochim. Acta, Part A*, 1998, **54**, 893.
25 K. Samanta, A. K. Arora and R. S. Kativar, *J. Phys. D: Appl. Phys.*, 2012, **45**, 1.
26 Z. Xiao, Y. Liu, J. Zhang, D. Zhao, Y. Lu, D. Shen and X. Fan, *Semicond. Sci. Technol.*, 2005, **20**, 796.
27 http://rruff.info/, accessed in January of 2014.
28 J. Huang, X. XU, C. Gu, W. Wang, B. Geng, Y. Sun and J. Liu, *Sens. Actuators, A*, 2012, **171–172**, 572.
29 T. J. Yan, X. X. Wang, J. L. Long, P. Liu, X. L. Fu, G. Y. Zhang and X. Z. Fu, *J. Colloid Interface Sci.*, 2008, **325**, 425.
30 W. H. Feng, Z. X. Pei, Z. B. Fang, M. L. Huang, M. L. Lu, S. X. Weng, Z. Y. Zheng, J. Hu and P. Liu, *J. Mater. Chem. A*, 2014, **2**, 7802.
31 O. F. Lopes, V. R. de Mendonça, F. B. F. Silva, E. C. Paris and C. Ribeiro, *Quim. Nova*, 2015, **38**, 106.
32 V. Kumari, A. K. Patra and A. Bhaumik, *RSC Adv.*, 2014, **4**, 13626.
33 V. R. de Mendonça, O. F. Lopes, R. P. Fregonesi, T. R. Giraldi and C. Ribeiro, *Appl. Surf. Sci.*, 2014, **298**, 182.
34 T. T. Vu, L. del Río, T. Valdés-Solís and G. Marbán, *Appl. Catal., B*, 2013, **140**, 189.
35 H. Fu, T. Xu, S. Zhu and Y. Zhu, *Environ. Sci. Technol.*, 2008, **42**, 8064.